Supporting information

A Highly Resilient, Conductive, and Anti-Swelling Hybrid-Crosslinked Hydrogel Based on a Semi-Interpenetrating Network for Multimodal Sensing and Marine Monitoring

Xiang Di[a,b], Yi Wang[a,b], Bo Yu [a,b], Weiqiang Ran [a,b], Ruotong Zhang[a,b], Xuefeng Gao[c], Chungang Yuan[a,b*]

[a]Yanzhao Electric Power Laboratory of North China Electric Power University, 071000, Baoding, China E-mail: cgyuan@ncepu.edu.cn; Fax: +86-312-7525509

[b]Hebei Key Laboratory of New Energy Environmental Safety and Resource Utilization, Department of Environmental Science and Engineering, North China Electric Power University, 071000, Baoding, China

[c]National Pesticide Engineering Research Center (Tianjin), College of Chemistry, Nankai University, 300071, Tianjin, China

Experimental Section/Methods

Materials

Sodium alginate (SA), potassium persulfate (KPS), and acrylamide (AM) were purchased from Aladdin Biochemical Technology Co., Ltd. (Shanghai, China). N,N-methylenebisacrylamide (MBAA) was obtained from Macklin Biochemical Technology Co., Ltd. (Shanghai, China). Anhydrous calcium chloride ($CaCl_2$) was supplied by Energy Chemical. The Ti_3AlC_2 powder was purchased from XINXI Technology Co., Ltd. All experiments were performed using deionized water.

Preparation of MXene ($Ti_3C_2T_x$) Nanosheets

First, 1 g LiF was dissolved in 20 mL of HCl solution. Then, 1 g Ti_3AlC_2 powders were slowly added into the above solution and stirred at 35 °C for 24 h. The mixture was then centrifuged with deionized water (3500 rpm, 5 min) and washed repeatedly until the pH value of the supernatant was greater than six. The precipitate was then ultrasonically exfoliated (60 min). Finally, the reaction solution was centrifuged at 3500 rpm for 1 h, and the upper solution was collected and freeze-dried to obtain the MXene.

Preparation of Hybrid Cross-Linked Hydrogels

A solution was first prepared by dissolving 1.5 g of AM in deionized water under stirring. Subsequently, 5 mg of MBAA, SA (at mass concentrations ranging from 2.5 to 10 mg/mL), and MXene (at mass concentrations of 0-4 mg/mL) were added to the solution. Finally, 20 mg of KPS was introduced into the mixture, which was then stirred and sonicated for 5 minutes. The resulting mixture was poured into a glass mold and allowed to polymerize at 60 °C for 5 hours to form the hydrogel. The obtained hydrogel was subsequently immersed in 0.1 mol/L $CaCl_2$ solution for 24 h. To systematically investigate the variations in material properties, the mass ratios of SA and MXene were adjusted during preparation. Detailed compositional parameters are provided in **Table S1.**

Characterization

The chemical structures of the various hydrogels were characterized using Fourier transform infrared (FTIR) spectroscopy (A225/Q Platinum ATR). X-ray diffraction (XRD) analysis was performed on a Rigaku Smart Lab diffractometer (Japan) with Cu-Kα radiation (λ = 1.5414 Å) to determine the crystallinity of the materials. The morphological features of the lyophilized hydrogels were observed using a scanning electron microscope (SEM, TM4000Plus II, Japan). For SEM observation, the hydrogels were freeze-dried, immersed in liquid nitrogen for 3 minutes, fractured, and mounted on carbon pads attached to the sample stage. The phase transition temperature of the hydrogels was determined by differential scanning calorimetry (DSC) at a heating/cooling rate of 5 °C·min^{-1} under a nitrogen atmosphere, over a temperature range of 25 to -55 °C.

Mechanical test

All mechanical tensile tests of the hydrogels were performed using a universal materials testing machine (Suns Technology Co., Ltd., China). The hydrogel samples were first cut into rectangular strips measuring 50 mm×4 mm×1 mm and tested at room temperature. Uniaxial tensile tests were conducted at a strain rate of 50 mm·min^{-1}, while cyclic loading–unloading tests were performed at a strain rate of 100 mm·min^{-1}. The Young's modulus was determined by calculating the slope of the stress-strain curve within the 5-20% strain range. Toughness was evaluated by integrating the area under

the stress-strain curve. The sample dimensions were accurately measured using a vernier caliper. To ensure reliability, at least five replicates were tested for each condition, and the results are reported as mean ± standard deviation.

Weight Swelling Rate test

The swelling ratio of the hydrogels was measured using the gravimetric method at room temperature (25 °C). The initial weight of the hydrogel sample, denoted as W_p, was recorded. The hydrogel was then immersed in deionized water, physiological saline, anhydrous ethanol, or acetone. At specified time intervals, the sample was removed, gently blotted dry to remove surface liquid, and weighed. This process was repeated until no significant change in weight was observed, indicating that swelling equilibrium had been reached. The swelling ratio was calculated using the following formula:

$$Swell\ ratio(\%) = \left(\frac{w_r - w_p}{w_p}\right) \times 100\%$$

where W_p represents the initial weight of the sample, and W_r denotes the weight at swelling equilibrium. For each condition, three parallel samples were tested, and the average value was reported as the final swelling ratio of the hydrogel.

Conductivity test

The electrical characterization of hydrogel was performed using a electrochemical workstation (CHI-660E, Chenhua Instruments) under various operational conditions. Electrical conductivity (σ) was determined through the fundamental relationship:

$$\sigma = \left(\frac{L}{AR}\right)$$

where L denotes the inter-electrode spacing (mm), A represents the effective contact area (mm²) between the hydrogel and electrodes, and R corresponds to the measured bulk resistance (Ω).

The normalized resistance variation, expressed as $\Delta R/R_0$ was quantified through continuous monitoring:

$$\frac{\Delta R}{R_0} = \left(\frac{R - R_0}{R_0}\right) * 100\%$$

where R_0 indicates the baseline resistance in unstrained conditions and ΔR reflects real-time resistance fluctuations during mechanical deformation.

The GF was defined as follows:

$$GF = \frac{\Delta R/R_0}{\varepsilon}$$

where $\Delta R/R_0$ is the change in relative resistance of the strain sensor and ε is the corresponding change in strain of the sample.

Rheological test

The viscoelastic response and self-recovery behavior of the hydrogels were investigated using a parallel-plate rheometer (TA Instruments DHR-2, 25 mm diameter plates). To minimize solvent evaporation during measurements, a thin layer of silicone oil was applied around the sample edges. Strain amplitude sweep tests (0.1–1000%) were conducted at a fixed frequency of 1 Hz to determine the linear viscoelastic region (LVR). Subsequently, frequency sweep measurements (0.1-100 rad/s) were performed within the LVR at a constant strain of 1% to characterize the viscoelastic moduli as a function of angular frequency.

Table S1. Recipes for hydrogels

Hydrogels	SA (mg)	MBAA (mg)	AM (g)	Mxene (mg/mL)	KPS (mg)	Water (mL)	$CaCl_2$ (mol/L)
$SA_{2.5}M_0$	12.5	10	1.5	0	20	5	0
SA_3M_0	15	10	1.5	0	20	5	0
SA_5M_0	25	10	1.5	0	20	5	0
$SA_{10}M_0$	50	10	1.5	0	20	5	0
$SA_3M_{0.5}$	15	10	1.5	0.5	20	5	0
SA_3M_1	15	10	1.5	1	20	5	0
SA_3M_2	15	10	1.5	2	20	5	0
SA_3M_3	15	10	1.5	3	20	5	0
SA_3M_2-Ca^{2+}	15	10	1.5	2	20	5	0.1

Table S2. Comparison of the tensile strain and electrical conductivity of hydrogels.

Sample	Conductivity (S/m)	Strain (%)	Source
SA_3M_2-Ca^{2+} hydrogel	1.44	778	This work
$PR_{0.1}$-IL-3 hydrogel	0.85	823.45	Ref.1[1]
I-CSCH hydrogel	0.32	560	Ref.2[2]
PVA/CNT-S hydrogel	0.11	320	Ref.3[3]
PADW4-Li hydrogel	0.3	700	Ref.4[4]
MXene/DES@PAM hydrogel	0.65	500	Ref.5[5]
0.4%-MCPP hydrogel	0.45	847	Ref.6[6]
PAS-3 hydrogel	0.17	1200	Ref.7[7]
$P_{10\%}B_{0.45\%}A_{10\%}$/K-100% hydrogel	1.33	838	Ref.8[8]
BA_2 hydrogel	0.689	696	Ref.9[9]
P(AA-$APA_{50.14}$)-Fe^{3+} hydrogel	0.55	880	Ref.10[10]

Table S3. Comparison of the resilience of hydrogels under different strain conditions.

Sample	Resilience (%)	Strain (%)	Source
SA_3M_2-Ca^{2+} hydrogel	99.5%	50	This work
AP_2 hydrogel	94	200	Ref.11[11]
APU-2 hydrogel	95.5	100	Ref.12[12]
EA-PR-IL-hydrogel	93	200	Ref.13[13]
PVA_{10}/$P(Iig)_{15}$ hydrogel	85	100	Ref.14[14]
$GMOH_x$ hydrogel	94	100	Ref.15[15]
poly(ACMO)/Pt	86.5	100	Ref.16[16]

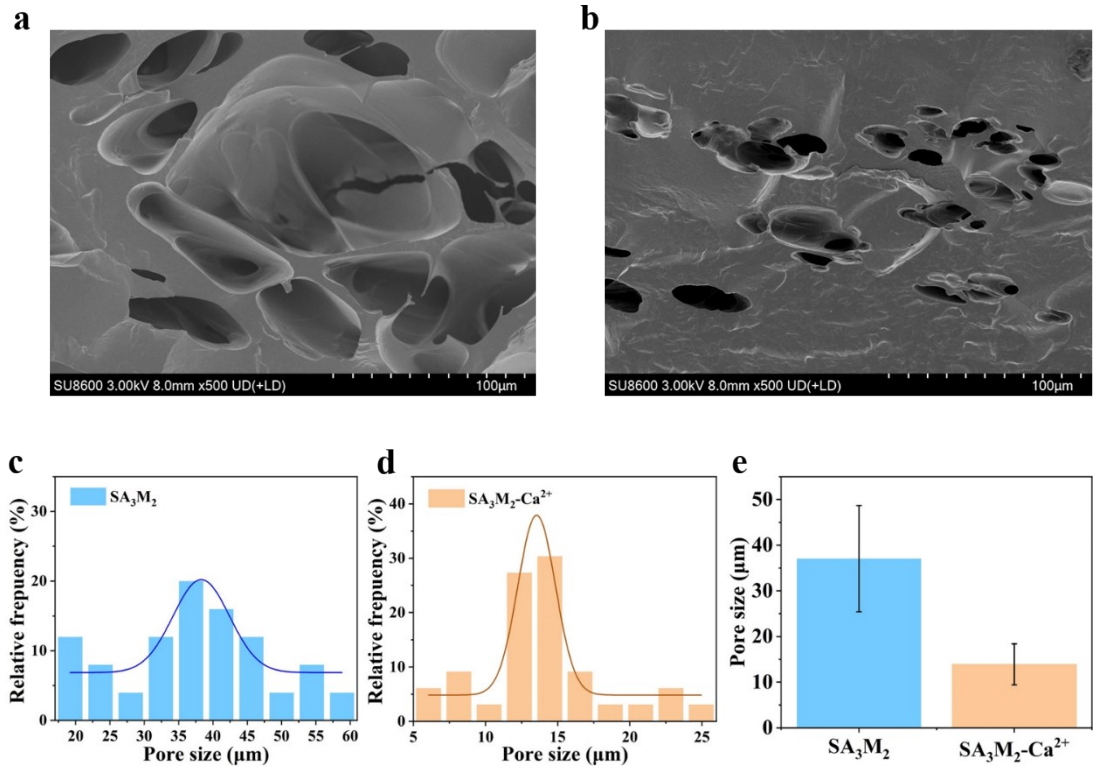

Figure S1. The SEM images of (a) SA_3M_2, and (b) SA_3M_2-Ca^{2+} gel. Relative frequency plots of (c) SA_3M_2 and (d) SA_3M_2-Ca^{2+} pore size distribution. (e) The pore size of SA_3M_2 and SA_3M_2-Ca^{2+} gels.

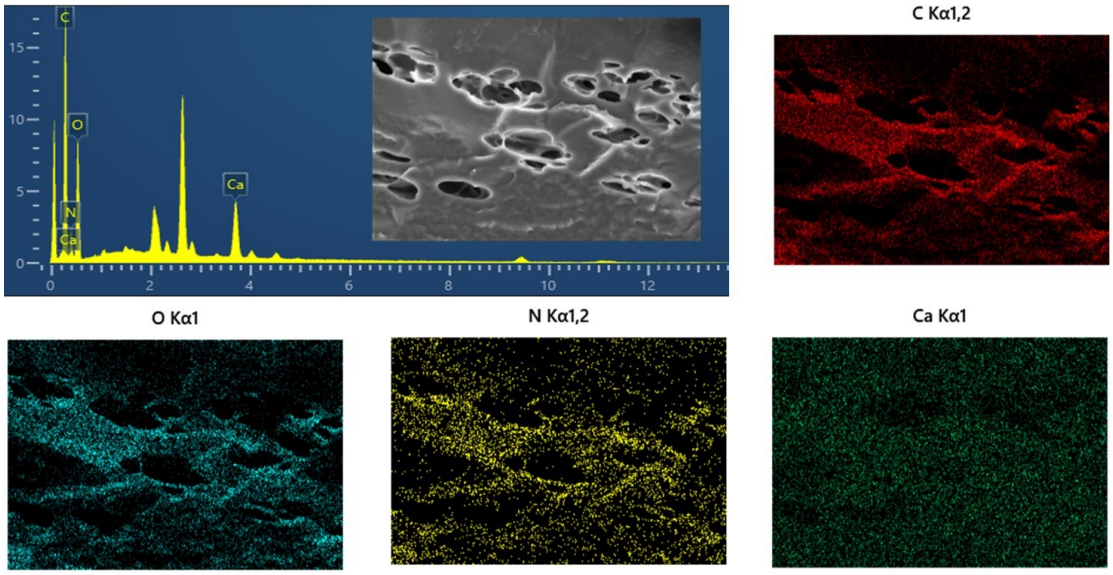

Figure S2. EDS images elemental maps for freeze-dried SA_3M_2-Ca^{2+} hydrogel.

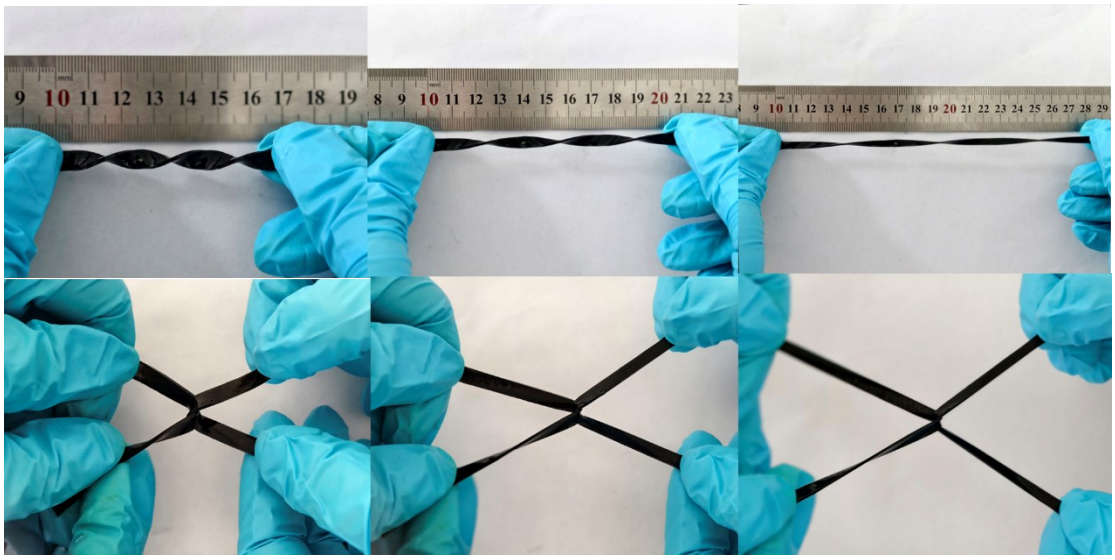

Figure S3. Mechanical performance of the hydrogel under twisting and cross-shaped stretching.

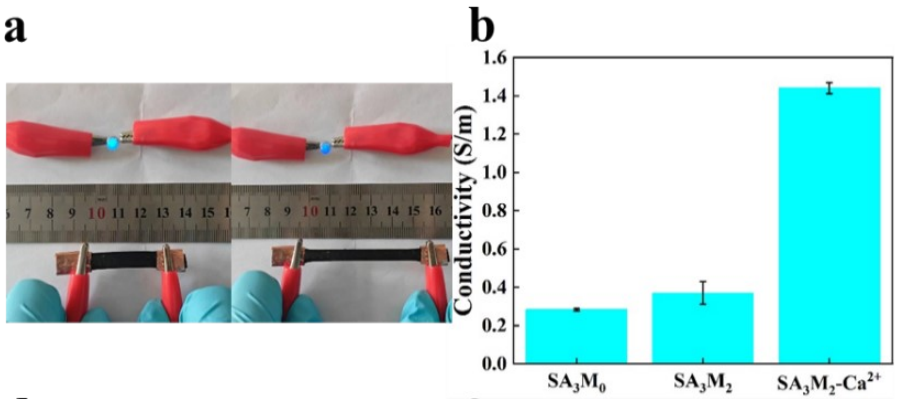

Figure S4. (a) Changes in LED brightness before and after stretching the hydrogel integrated into a circuit. (b) Electrical conductivity of hydrogels with different compositions.

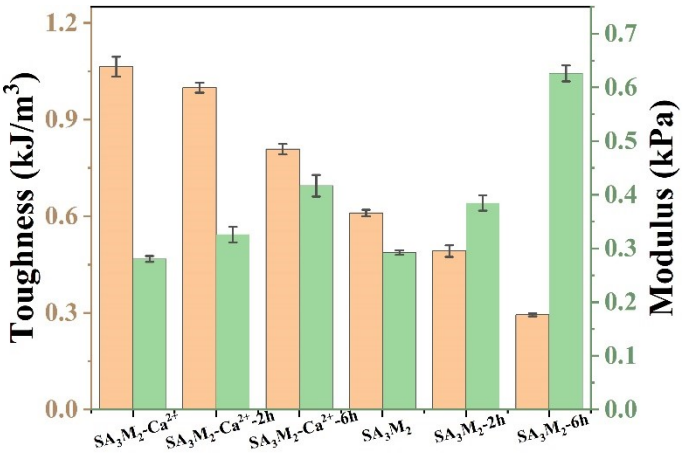

Figure S5. Comparison of toughness and elastic modulus between SA_3M_2-Ca^{2+}

and SA_3M_2 hydrogels after swelling.

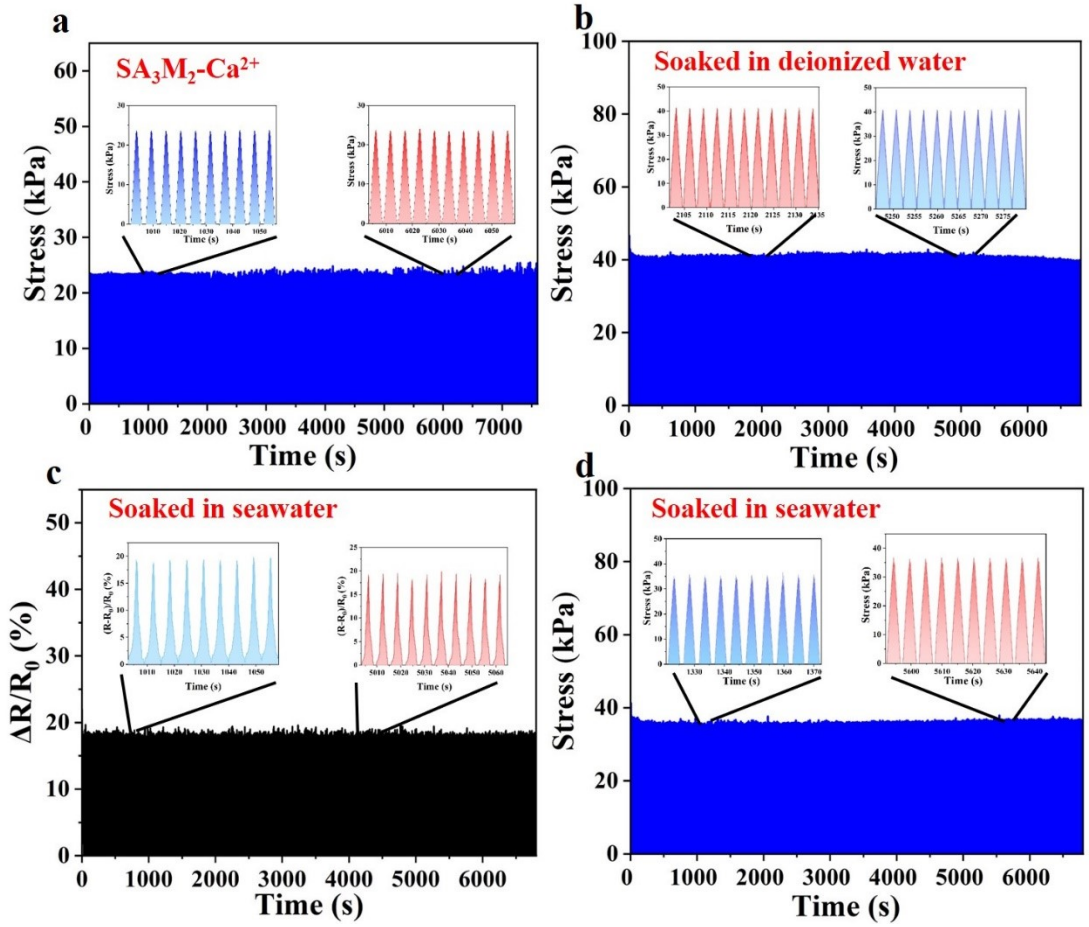

Figure S6. (a)Stress change of the hydrogel during 1500 electrical cycling tests. (b) The stress response of the hydrogel (immersed in deionized water for 15 days) under 1500 tensile cycles at 50% strain. (c) Relative resistance change and (d) stress change of the hydrogel (immersed in artificial seawater for 15 days) under 1500 tensile cycles at 50% strain

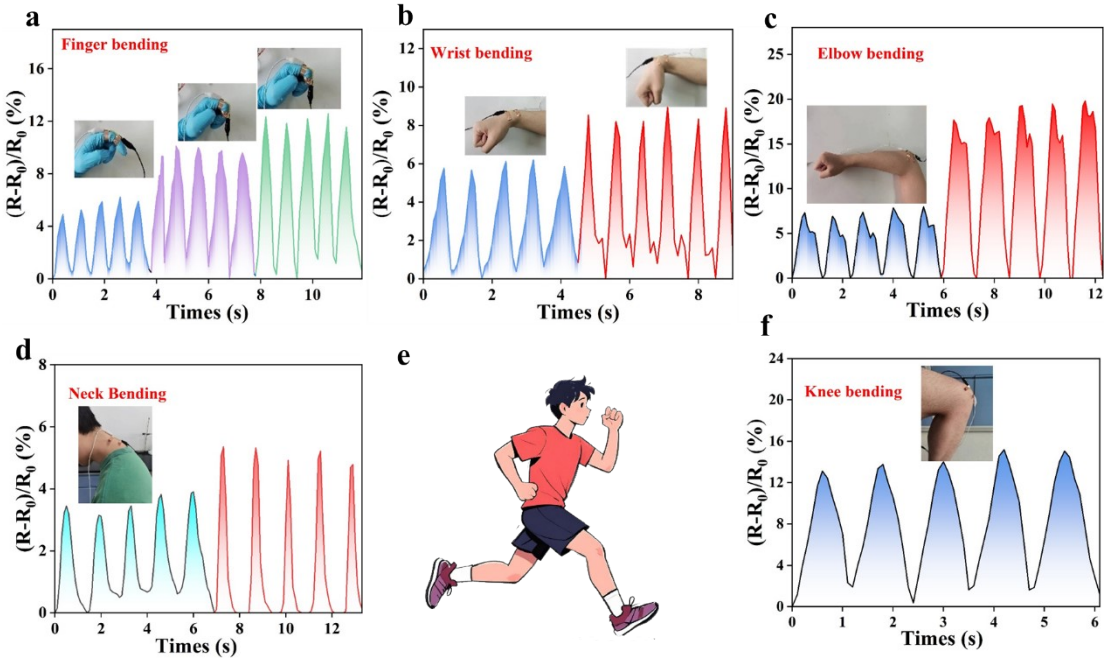

Figure S7. Demonstration of the hydrogel-based sensor for monitoring various human joint movements. The sensor was attached to different body parts to detect motions of the (a) finger, (b) wrist, (c) elbow, (d) neck, and (f) knee. (e) A schematic diagram shows the potential application of the sensor in wearable health monitoring systems.

A •—	B —•••	C —•—•	D —••
E •	F ••—•	G ——•	H ••••
I ••	J •———	K —•—	L •—••
M ——	N —•	O ———	P •——•
Q ——•—	R •—•	S •••	T —
U ••—	V •••—	W •——	X —•—•
Y —•——	Z ——••	1 •————	2 ••———
3 •••——	4 ••••—	5 •••••	6 —••••
7 ——•••	8 ———••	9 ————•	0 —————

Figure S8. Morse code chart and its corresponding signal representations.

References

1. Bai, Y.; Xie, S.; Yan, S.; Li, X., Conductive Poly(Ionic Liquid) Hydrogel for Human-Machine Interfaces, Underwater Communication and Rescue Alarm. *Chem. Eng. J.* **2026,** *528*, 172417.
2. Xu, M.; Li, C.; Ban, Q.; Wang, W.; Gu, Z.; Xu, H., Encapsulated Structural Color Hydrogel Composite with Tough Interface for High-Sensitive Dual-Mode Underwater Sensing,Communication and Tissue Monitoring. *Chem. Eng. J.* **2025,** *526*, 170838.
3. Li, S.; Ma, J.; Zhu, C.; Chen, G.; Han, J.; Fu, J., Anisotropic Tough and Non-Swelling Hydrogels Based on Hofmeister-Effect for Underwater Monitoring. *Adv. Funct. Mater.* **2025**, e27007.
4. Song, Y.; Yang, M.; Liu, T.; Sun, C.; Jin, M.; Tan, H.; Zheng, D.; Zhang, Y., Design of A Flexible Cellulose Framework via Supramolecular Structure Modulation and Its Application in Hydrogel Sensors. *Carbohydr. Polym.* **2026,** *373*, 124591.
5. Liu, Z.; Wang, D.; Liu, G.; Zhang, H.; Li, H.; Li, X.; Wang, R., Sound-Bioinspired Dual-Conductive Hydrogel Sensors for High Sensitivity and Environmental Weatherability. *Chin. J. Struct. Chem.* **2025,** *44* (8), 100628.
6. Fu, Y.; Zou, J.; Wang, Y.; Yao, Z.; Lv, P.; Wu, D.; Wei, Q.; Zhang, W.; Jiang, Y.; Li, D., Highly Stretchable, Self-Adhesive, Conductive, and Tough Hydrogel Reinforced with Cellulose Nanofibers for Wearable Biosensor and Ultrasonic Nanogenerator. *Chem. Eng. J.* **2025,** *516*, 164010.
7. Zhang, S.; Hui, C.; Lu, S.; Xiao, J.; Jiang, L.; Wang, M.; Gan, D., Multifunctional Eutectogels with Environmental Tolerance for Intelligent Human–Machine Interfaces and Solid-State Energy Storage. *Chem. Eng. J.* **2025,** *525*, 169941.
8. Lei, L.; Hu, S.; Xie, Y.; Liu, X.; Xie, C.; Li, H., Synergistic Stretching-Annealing and Salting-Out Enabling Ultrastrong, Ultratough Anisotropic Bacterial Cellulose Conductive Hydrogels for Bioelectric Sensors. *Carbohydr. Polym.* **2026,** *371*, 124513.
9. Ara, L.; Khan, M.; Ullah, R.; Shah, L. A., Hydrophobically Associated Ionic Conductive Hydrogels as Strain, Pressure, and An Electronic Sensor for Human Motions Detection. *Sens. Actuators, A* **2023,** *362*, 114618.
10. Shen, K.; Xu, K.; Zhang, M.; Yu, J.; Yang, Y.; Zhao, X.; Zhang, Q.; Wu, Y.; Zhang, Y.; Cheng, Y., Multiple Hydrogen Bonds Reinforced Conductive Hydrogels with Robust Elasticity and Ultra-Durability as Multifunctional Ionic Skins. *Chem. Eng. J.* **2023,** *451*, 138525.
11. Wu, Y.; Zeng, F.; Ke, Y.; He, X.; Zhong, Z.; Sun, Z.; Xu, J., High-conductivity PBFDO-based self-adhesive hydrogel for low-hysteresis flexible sensing applications. *Polymer* **2025,** *336*, 128876.
12. Sun, B.; Liu, K.; Wu, B.; Sun, S.; Wu, P., Low-Hysteresis and Tough Lonogels via Low-Energy-Dissipating Cross-Linking. *Adv. Mater.* **2024,** *36* (44), 2408826.
13. Du, R.; Bao, T.; Zhu, T.; Zhang, J.; Huang, X.; Jin, Q.; Xin, M.; Pan, L.; Zhang, Q.; Jia, X., A Low-Hysteresis and Highly Stretchable Ionogel Enabled by Well Dispersed Slidable Cross-Linker for Rapid Human-Machine Interaction. *Adv. Funct. Mater.* **2023,** *33* (30), 2212888.

14. Zhang, M.; Yang, Y.; Li, M.; Shang, Q.; Xie, R.; Yu, J.; Shen, K.; Zhang, Y.; Cheng, Y., Toughening Fouble-Network Hydrogels Bypolyelectrolytes. *Adv. Mater.* **2023,** *35* (26), 2301551.
15. Zou, J.; Jing, X.; Li, S.; Feng, P.; Chen, Y.; Liu, Y., MXene crosslinked hydrogels with low hysteresis conferred by sliding tangle island strategy. *Small* **2024,** *20* (35), 2401622.
16. Guo, B.; Zhong, Y.; Chen, X.; Yu, S.; Bai, J., 3D Printing of Electrically Conductive and Degradable Hydrogel for Epidermal Strain Sensor. *Compos. Commun.* **2023,** *37*, 101454.